Journal of Advanced Research (2014) 5, 357–366

Cairo University

Journal of Advanced Research

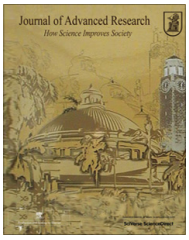

ORIGINAL ARTICLE

Chemical kinetic simulation of kerosene combustion in an individual flame tube

Wen Zeng *, Shuang Liang, Hai-xia Li, Hong-an Ma

Liaoning Key Lab of Advanced Test Technology for Aerospace Propulsion System, Shenyang Aerospace University, Shenyang, Liaoning 110136, PR China

ARTICLE INFO

Article history:
Received 20 April 2013
Received in revised form 4 June 2013
Accepted 4 June 2013
Available online 11 June 2013

Keywords:
Reduced reaction mechanism
Surrogate fuel
n-decane
Simulation
Combustion
Individual flame tube

ABSTRACT

The use of detailed chemical reaction mechanisms of kerosene is still very limited in analyzing the combustion process in the combustion chamber of the aircraft engine. In this work, a new reduced chemical kinetic mechanism for fuel *n*-decane, which selected as a surrogate fuel for kerosene, containing 210 elemental reactions (including 92 reversible reactions and 26 irreversible reactions) and 50 species was developed, and the ignition and combustion characteristics of this fuel in both shock tube and flat-flame burner were kinetic simulated using this reduced reaction mechanism. Moreover, the computed results were validated by experimental data. The calculated values of ignition delay times at pressures of 12, 50 bar and equivalence ratio is 1.0, 2.0, respectively, and the main reactants and main products mole fractions using this reduced reaction mechanism agree well with experimental data. The combustion processes in the individual flame tube of a heavy duty gas turbine combustor were simulated by coupling this reduced reaction mechanism of surrogate fuel *n*-decane and one step reaction mechanism of surrogate fuel $C_{12}H_{23}$ into the computational fluid dynamics software. It was found that this reduced reaction mechanism is shown clear advantages in simulating the ignition and combustion processes in the individual flame tube over the one step reaction mechanism.

Introduction

Detailed chemical kinetic simulation of the combustion process in the combustion chamber of the aircraft engine is very complex and still challenging. Kerosene is a mixture of hundreds, if not thousands, of hydrocarbons [1]. It is processed to meet a specification that covers a broad range of physical and chemical properties that include boiling range/volatility, heat of combustion, and freeze point. There is also a limit on the aromatic compounds concentrations in this fuel [2]. Development of chemical kinetic model for kerosene is a formidable task given its complex composition. Furthermore, although the detailed chemical kinetic mechanism can be developed for kerosene, coupling such detailed reaction mechanism into simulation of the combustion process in the combustion chamber of the practical aircraft engine is difficult due to the significant long computational time varying from a few days to several weeks. One possible way to solve this problem is to develop a surrogate fuel [3] for kerosene based

* Corresponding author. Tel.: +86 2489723722; fax: +86 2489723720.
E-mail address: zengwen928@sohu.com (W. Zeng).
Peer review under responsibility of Cairo University.

2090-1232 © 2013 Production and hosting by Elsevier B.V. on behalf of Cairo University.
http://dx.doi.org/10.1016/j.jare.2013.06.002

on chemical class distribution and by matching physical properties such as volatility, density, boiling point, and molecular weight and develop a relative simple reaction mechanism for this surrogate fuel. Accordingly, the structure of the aircraft engine combustion chamber must be simplified.

Surrogate fuels are defined as mixtures of a few hydrocarbon compounds whose physical (formation enthalpy, boiling, critical points, etc.) and chemical (C/H ratio, fuel ignition, fuel sooting tendency, etc.) properties pertinent to those of commercial fuels. Various hydrocarbons, e.g., *n*-decane, toluene, ethylbenzene, and cyclohexane were reported extensively in the literatures as the components of surrogate fuels for kerosene. Considerable detailed reaction mechanisms were also developed for these surrogate fuels in order to predict their ignition and combustion characteristics [4]. Vovelle et al. [5] used a surrogate mixture of 90 vol.% *n*-decane and 10 vol.% toluene to reproduce the oxidation of kerosene in the premixed burner, and the detailed mechanism including 207 reversible reactions and 39 species was adopted. This mechanism gave a good agreement between the computed and the experimental mole fractions of most of the species. Lindstedt and Maurice [6] formulated a TR0 surrogate mixture containing *n*-decane-benzene or toluene, or ethylbenzene, or ethylbenzene-naphtalene. The combustion process of this mixture was modeled using a detailed mechanism, including 1085 reversible reactions and 193 species, and the computed concentration profiles versus distance to the burner fit the experimental results with a precision compatible with the experimental uncertainties. Cathonnet et al. [7] used a detailed mechanism, including 1463 reversible reactions and 188 species, for a surrogate fuel containing 78% *n*-decane, 9.8% cyclohexane, and 12.2% toluene by volume, to simulate the combustion process of kerosene TR0 in JSR, and concentration profiles versus temperature were modeled. The major and minor species were simulated correctly. However, benzene formation was under-predicted.

The detailed kinetic modeling of kerosene oxidation was initially performed using *n*-decane as a surrogate fuel, since *n*-decane and kerosene had very similar oxidation rates and flame conditions [8,9]. A surrogate fuel containing only *n*-decane was used by Cathonnet et al. [10] to simulate the combustion process of kerosene TR0 in JSR at atmospheric pressure. A detailed mechanism including 603 reversible reactions and 78 species was developed for this fuel. Compared with the experimental results, the major species concentration profiles versus time were modeled correctly. Dagaut et al. [11] also used a detailed mechanism including 573 reversible reactions and 90 species for a surrogate fuel containing only *n*-decane to simulate the combustion process of kerosene TR0 in JSR at 10–40 atm pressure, and the major species concentration profiles versus temperature were modeled correctly. However, although using the single *n*-decane as the surrogate fuel for kerosene, the detailed reaction mechanism is still too complicated to be incorporated into computational fluid dynamic codes in simulating the combustion process of a practical combustor. These limitations forced scientists to develop reduced reaction mechanism by decreasing the numbers of chemical species and reactions without penalizing predictive qualities of the detailed reaction mechanism [12].

In the previous studies, the CFD software FLUENT always be used to simulate the combustion process in the aero-engine combustor. However, as the surrogate fuel of kerosene, only fuel $C_{12}H_{23}$ has been listed in the fuel database of this software, and the reaction mechanism of this surrogate fuel was very simple (one step reaction mechanism). The computed results such as temperature and emissions concentrations at the outlet of combustor were always different from the experimental data. So, in this article, firstly, we select fuel *n*-decane as a surrogate fuel for kerosene and develop a new reduced reliable reaction mechanism for this surrogate fuel, including 210 elemental reactions (including 92 reversible reactions and 26 irreversible reactions) and 50 species. Secondly, the ignition and combustion characteristics of this surrogate fuel in the shock tube and flat-flame burner, respectively, are simulated using this reduced mechanism, and the results are compared with the simulated results by using the detailed mechanism and the experimental data. Lastly, coupling this reduced reaction mechanism into CFD software (FLUENT), the combustion process in the individual flame tube of a heavy duty gas turbine combustor is kinetic simulated.

Methodology

*Detailed reaction mechanism for **n**-decane*

Leclerc and his co-workers [13] simulated the combustion processes of fuel *n*-decane in a jet-stirred reactor [14] and a premixed laminar flame [15]. Their mechanism, generated automatically, included a massive 7920 reactions. Zeppieri et al. [16] developed a partially reduced mechanism for the oxidation and pyrolysis of *n*-decane, and it was validated against flow reactor, jet-stirred reactor, and *n*-decane/air shock tube ignition delay [17] data. The approach included detailed chemistry of *n*-decane and the five *n*-decyl radicals, and it also combined both internal hydrogen isomerization reactions and β-scission pathways for the various system radicals.

Bikas and Peters [18] developed a chemical kinetic mechanism for *n*-decane. This chemical kinetic mechanism was previously validated using experimental data obtained from shock tubes, jet-stirred reactor, stabilized premixed flame, and a freely propagating premixed flame [19]. The good agreements between predictions and the experimental data obtained in the jet-stirred reactor, stabilized premixed flame, and freely propagating premixed flame were obtained. Ignition delay times calculated using this reaction mechanism agreed with experimental data obtained in shock tubes in the high temperature regime, while little discrepancies were observed in the intermediate and low temperature regime. This reaction mechanism was also validated with experimental auto-ignition data obtained in a counter-flow burner under non-premixed conditions. Following considerable modifications were made by Honnet et al. to this chemical kinetic mechanism to improve agreement with previous ignition delay time measured at low temperature in the shock tube [4]. These changes were necessary to obtain better predictions of auto-ignition of this type of surrogate fuel.The present study is begun with the detailed chemical kinetic mechanism proposed by Bikas and Peters (BP). The BP mechanism consists of 67 chemical species and 631 elemental reactions (including 265 reversible reactions and 101 irreversible reactions). At the same time, some modifications are made to this mechanism according to the report by Honnet et al. [4]. In the chemical kinetic mechanism, the rate constants k_f of the elementary reactions are calculated using the expression $k_{fk} = A_k T^{\beta_k} \exp[-E_{ak}/(RT)]$, where T is the temperature, R is the universal gas constant.

The quantities A_k, β_k, and E_{ak} are, respectively, pre-exponential constant, the temperature exponent, and the activation energy of the elementary reaction k. According to modifications by Honnet et al., the values of A for some elementary reactions in BP chemical kinetic mechanism were modified, while the values of β and E were the same. The numbers of species and reactions were also not changed. These modifications were reported previously in details [4].

Reduced reaction mechanism for n-decane

However, the detailed reaction mechanism is too complicated. If we want to combine this complicated reaction mechanism with computational fluid dynamic codes (such as Fluent) to simulate the combustion process in the practical combustor (such as aero-engine), this size inflation of detailed kinetic mechanism requires significant computational time (from a few days to several weeks). Thus, simplification is performed to derive a more valid and general mechanism for the whole combustion domain. The potentially redundant species and reactions without decreasing predictive capacities of the detailed mechanism are eliminated. Although the simplifications can be achieved from various ways including lumped parameter method (LP) [20], sensitivity analysis (SA), and time scale analysis (TSA), only sensitivity analysis is used in the current study [21].

Sensitivity analysis is a powerful and systematic way to determine quantitatively the relationship between the solution to a model and the various parameters that appear in the model's definition.

The system of ordinary differential equations that describe the physical problem is of the general form:

$$dZ/dt = F(Z, t, a) \tag{1}$$

where in our case, $Z = (T, Y_1, Y_2, \ldots, Y_i)^t$ is the vector of temperature and mass fractions, $a = (A_1, A_2, \ldots, A_k)$ is the pre-exponential constant of any reactions.

The first-order sensitivity coefficient matrix is defined as:

$$w_{l,i} = \partial Z_l/\partial a_i \tag{2}$$

where the indices l and i refer to the dependent variables and reactions, respectively. Differentiating Eq. (2) with respect to the parameters a_i yields:

$$\frac{dw_{l,i}}{dt} = \frac{\partial F_l}{\partial Z} \cdot w_{l,i} + \frac{\partial F_l}{\partial a_i} \tag{3}$$

Eq. (3) is linear in the sensitivity coefficients, even if the model problem is nonlinear. This equation is added to Eq. (2) and is numerically solved by an integrator like DASSL. The solution of Eq. (3) supplies the sensitivities of each state variable Z_i to each parameter a_j as a function of time t. Sensitivities for the ignition delay time can be obtained from the definition of the ignition delay time, as the time where the temperature reaches a certain level T^*, in our calculations, is 1500 K:

$$T(\tau; a) - T^* = 0 \tag{4}$$

Implicit differentiation of this equation gives the desired sensitivity of the ignition delay time:

$$\partial\tau/\partial a_j = -\left(\left.\frac{\partial T}{\partial a_j}\right|_{t=\tau}\right) \Big/ \left(\left.\frac{\partial T}{\partial t}\right|_{t=\tau}\right) \tag{5}$$

The sensitivities of the temperature $\partial T/\partial a_j$ are calculated from Eq. (3) and evaluate at $t = \tau$, as well as the source term of the energy equation $\partial T/\partial t$.

The complexity of the reaction mechanism is depended on the selection of sensitivity coefficients. The number of reactions (also species) is decreased with sensitivity coefficients selected increasing. If these sensitivity coefficients selected are too large, some reactions whose sensitivity coefficients are little but have effect on the fuel ignition and combustion characteristics will be removed. However, if these sensitivity coefficients selected are too little, the number of reactions (also species) is increased greatly. In this paper, our aim is to combine this reduced reaction mechanism with computational fluid dynamic code-Fluent to simulate the combustion process in the practical combustor (such as aero-engine). The computational fluid dynamic code-Fluent can compute the number of species is not more than fifty. So, for the sake of furthest reflect the predictive capacities of the detailed mechanism and the number of species is not more than fifty, in sensitivity analysis for the ignition delay time, we choose those reactions whose sensitivity coefficients exceeding 2.0, and in sensitivity analysis for species concentrations, we choose reactions whose sensitivity coefficients larger than 0.01. Combining the results of these two sensitivity analysis can lead to a reduced mechanism of fuel *n*-decane.

Table 1 summarizes the crucial results from the sensitivity analyses conducted for the detailed mechanism of *n*-decane. As can be seen from the table, the reduced mechanism is characterized by 50 species and 210 elementary reactions (including 92 reversible reactions and 26 irreversible reactions).

Ignition delay time in the shock tube

According to the experiment described in Ref. [18], the ignition delay times calculated at pressures of 12 and 50 bar using the detailed and reduced mechanisms are plotted in Fig. 1. At each value of the pressure, calculations performed for equivalence ratio are 1.0 and 2.0, respectively.

In Fig. 1, the solid lines donate the results obtained by the detailed mechanism, while the double dotted lines represent the calculations from the reduced mechanism. The symbols stand for the experimental data described in Ref. [18]. It is noted that the ignition delay times calculated from the reduced mechanism agree well with the experimental data and those from the detailed mechanism.

Premixed combustion in the premixed burner

It is generally recognized that premixed laminar flames constitute an attractive medium in which to study combustion chemistry. Such flames retain important transport features, which are not discernible in spatially homogeneous reactors. Therefore, this reduced mechanism is evaluated in comparison with the detailed mechanism computed and experimental profiles for major, stable intermediate, and radical species in laminar premixed flame stabilized in the flat-flame burner.

In experiment described in Ref. [22], the fuel was kerosene Jet-A1 containing 79 vol.% *n*-alkanes, 10 vol.% cycloalkanes

Table 1 Elementary reactions for *n*-decane reduced mechanism.

Reaction	*A* (mole cm s)	*E* (cal/mole)	Reaction	*A* (mole cm s)	*E* (cal/mole)
$H + O_2 \Longleftrightarrow OH + O$	9.756e+13	14842.26	$C_2H_4 + OH \Longleftrightarrow C_2H_3 + H_2O$	3.000e+13	3011.47
$O + H_2 \Longleftrightarrow OH + H$	5.119e+04	6285.85	$C_2H_4 + O \Longleftrightarrow CH_3 + HCO$	1.355e+07	178.78
$OH + H2 \Longleftrightarrow H_2O + H$	1.024e+08	3298.28	$C_2H_5(+M) \Rightarrow C_2H_4 + H(+M)$	8.200e+13	39913.96
$2OH \Longleftrightarrow H_2O + O$	1.506e+09	100.38	$C_2H_4 + H(+M) \Rightarrow C_2H_5(+M)$	3.975e+09	1290.63
$H + O_2 + M \Longleftrightarrow HO_2 + M$	3.535e+18	0.00	$C_2H_5 + O_2 \Longleftrightarrow C_2H_4 + HO_2$	1.024e+10	2186.90
$HO_2 + H \Longleftrightarrow 2OH$	1.686e+14	874.76	$C_2H_6 + H \Longleftrightarrow C_2H_5 + H_2$	1.400e+09	7433.08
$HO_2 + H \Longleftrightarrow H_2 + O_2$	4.276e+13	1410.13	$C_2H_6 + OH \Longleftrightarrow C_2H_5 + H_2O$	7.200e+06	860.42
$HO2 + H \Longleftrightarrow H_2O + O$	3.011e+13	1720.84	$C_2H_2 + {}_1\text{-}CH_2 \Longleftrightarrow C_3H_3 + H$	1.800e+14	0.00
$2\,HO_2 \Longleftrightarrow H_2O_2 + O_2$	5.200e+12	1539.20	$C_3H_3 + O \Longleftrightarrow CH_2O + C_2H$	2.000e+13	0.00
$H_2O_2(+M) \Longleftrightarrow 2OH(+M)$	2.494e+20	52376.75	$C_3H_3 + O \Longleftrightarrow C_2H_2 + CO + H$	1.400e+14	0.00
$CO + OH \Longleftrightarrow CO_2 + H$	8.970e+06	−740.92	$C_3H_6 + H \Longleftrightarrow C_3H_5 + H_2$	5.000e+12	1505.74
$CO + HO_2 \Longleftrightarrow CO_2 + OH$	1.510e+14	23637.67	$C_3H_6 + CH_3 \Longleftrightarrow C_3H_5 + CH_4$	8.960e+12	8508.60
$HCO + M \Longleftrightarrow CO + H + M$	7.000e+14	16802.10	$C_3H_6 + OH \Longleftrightarrow C_2H_5 + CH_2O$	7.900e+12	0.00
$HCO + H \Longleftrightarrow CO + H_2$	9.033e+13	0.00	${}_n\text{-}C_3H_7 \Longleftrightarrow CH_3 + C_2H_4$	9.600e+13	31022.94
$HCO + OH \Longleftrightarrow CO + H_2O$	1.024e+15	0.00	${}_n\text{-}C_3H_7 \Longleftrightarrow H + C_3H_6$	1.250e+14	37021.99
$HCO + O_2 \Longleftrightarrow CO + HO_2$	3.011e+12	0.00	$C_2H_5 + CH_3 \Longleftrightarrow C_3H_8$	7.000e+12	0.00
$CH + H_2 \Longleftrightarrow H + {}_3\text{-}CH_2$	1.110e+08	1673.04	$C_3H_8 + H \Longleftrightarrow {}_n\text{-}C_3H_7 + H_2$	1.300e+14	9703.63
${}_3\text{-}CH_2 + CH_3 \Longleftrightarrow C_2H_4 + H$	4.215e+13	0.00	$C_2H_2 + C_2H \Longleftrightarrow {}_u\text{-}C_4H_3$	1.200e+12	0.00
${}_3\text{-}CH_2 + O_2 \Rightarrow CO + OH + H$	1.300e+13	1481.84	${}_u\text{-}C_4H_3 + O_2 \Rightarrow C_2H + 2HCO$	1.000e+12	2007.65
${}_3\text{-}CH_2 + O_2 \Rightarrow CO_2 + H_2$	1.200e+13	1481.84	$C_4H_4 + H \Longleftrightarrow {}_u\text{-}C_4H_3 + H_2$	1.500e+14	10205.54
${}_1\text{-}CH_2 + M \Longleftrightarrow {}_3\text{-}CH_2 + M$	1.500e+13	0.00	$C_4H_4 + OH \Longleftrightarrow {}_u\text{-}C_4H_3 + H_2O$	7.000e+13	3011.47
${}_1\text{-}CH_2 + H_2 \Longleftrightarrow CH_3 + H$	7.227e+13	0.00	$C_2H_2 + C_2H_3 \Longleftrightarrow {}_u\text{-}C_4H_5$	1.200e+12	0.00
${}_1\text{-}CH_2 + O_2 \Rightarrow CO + OH + H$	3.130e+13	0.00	$C_4H_4 + H \Longleftrightarrow {}_s\text{-}C_4H_5$	5.500e+12	2390.06
${}_1\text{-}CH_2 + C_2H_4 \Longleftrightarrow C_3H_6$	9.635e+13	0.00	$C_4H_4 + H \Longleftrightarrow {}_u\text{-}C_4H_5$	5.500e+12	2390.06
${}_1\text{-}CH_2 + CO_2 \Longleftrightarrow CO + CH_2O$	1.400e+13	0.00	${}_u\text{-}C_4H_5 + M \Longleftrightarrow {}_s\text{-}C_4H_5 + M$	1.000e+14	0.00
$CH_2O + H \Rightarrow HCO + H_2$	1.260e+08	2165.39	${}_u\text{-}C_4H_5 + O_2 \Rightarrow C_2H_3 + CO + CH_2O$	1.000e+12	2007.65
$CH_2O + OH \Rightarrow HCO + H_2O$	3.433e+09	−454.11	$C_3H_3 + CH_3 \Rightarrow C_4H_6$	2.000e+12	0.00
$2CH_3 \Longleftrightarrow C_2H_5 + H$	3.160e+13	14674.95	$C_4H_6 + H \Longleftrightarrow {}_s\text{-}C_4H_5 + H_2$	3.000e+07	5999.04
$2CH_3(+M) \Rightarrow C_2H_6(+M)$	1.813e+13	0.00	$C_4H_6 + OH \Longleftrightarrow {}_u\text{-}C_4H_5 + H_2O$	2.000e+07	4995.22
$CH_3 + O \Longleftrightarrow CH_2O + H$	8.430e+13	0.00	$C_4H_6 + OH \Longleftrightarrow {}_s\text{-}C_4H_5 + H_2O$	2.000e+07	2007.65
$OH + CH_3 \Longleftrightarrow {}_1\text{-}CH_2 + H_2O$	2.500e+13	0.00	$C_4H_6 + OH \Longleftrightarrow C_2H_3 + CH_3CHO$	5.000e+12	0.00
$CH_3 + HO_2 \Longleftrightarrow CH_3O + OH$	3.780e+13	0.00	$C_4H_7 \Longleftrightarrow C_4H_6 + H$	1.200e+14	49330.78
$CH_3 + O_2 \Longleftrightarrow CH_2O + OH$	3.300e+11	8938.81	$C_4H_7 \Longleftrightarrow C_2H_4 + C_2H_3$	1.000e+11	37021.99
$CH_3 + H(+M) \Longleftrightarrow CH_4(+M)$	2.108e+14	0.00	$C_4H_7 + O_2 \Longleftrightarrow C_4H_6 + HO_2$	1.000e+11	0.00
$CH_3O + M \Rightarrow CH_2O + H + M$	5.420e+13	13503.82	$C_4H_7 + CH_3 \Longleftrightarrow C_4H_6 + CH_4$	1.000e+13	0.00
$CH_4 + H \Longleftrightarrow CH_3 + H_2$	1.300e+04	8030.59	$C_4H_7 + C_3H_5 \Longleftrightarrow C_4H_6 + C_3H_6$	4.000e+13	0.00
$CH_4 + O \Longleftrightarrow CH_3 + OH$	7.227e+08	8484.70	$C_3H_5 + CH_3 \Longleftrightarrow {}_1\text{-}C_4H_8$	1.000e+13	0.00
$CH_4 + OH \Longleftrightarrow CH_3 + H_2O$	1.560e+07	2772.47	${}_1\text{-}C_4H_8 + H \Longleftrightarrow C_4H_7 + H_2$	5.000e+13	3895.79
$C_2H + O_2 \Longleftrightarrow HCCO + O$	1.800e+13	0.00	${}_1\text{-}C_4H_8 + O \Longleftrightarrow CH_3 + C_2H_5 + CO$	1.625e+13	860.42
$HCCO + H \Longleftrightarrow {}_1\text{-}CH_2 + CO$	1.500e+14	0.00	${}_1\text{-}C_4H_8 + O \Longleftrightarrow C_3H_6 + CH_2O$	7.230e+05	−1051.63
$HCCO + O_2 \Longleftrightarrow HCO + CO_2$	8.130e+11	855.64	${}_1\text{-}C_4H_8 + OH \Longleftrightarrow {}_n\text{-}C_3H_7 + CH_2O$	6.500e+12	0.00
$HCCO + O_2 \Longleftrightarrow 2CO + OH$	8.130e+11	855.64	${}_p\text{-}C_4H_9 \Longleftrightarrow C_2H_5 + C_2H_4$	2.500e+13	28824.09
$C_2H_2 + O_2 \Longleftrightarrow HCCO + OH$	2.000e+08	30114.72	${}_p\text{-}C_4H_9 \Longleftrightarrow {}_1\text{-}C_4H_8 + H$	1.260e+13	38623.33
$C_2H_2 + H \Longleftrightarrow C_2H + H_2$	6.620e+13	27724.67	$C_5H_9 \Rightarrow C_3H_5 + C_2H_4$	2.500e+13	30019.12
$C_2H_2 + OH \Longleftrightarrow C_2H + H_2O$	3.380e+07	13986.62	$C_5H_9 \Rightarrow C_2H_3 + C_3H_6$	2.500e+13	30019.12
$C_2H_2 + O \Longleftrightarrow {}_3\text{-}CH_2 + CO$	2.168e+06	1570.27	${}_1\text{-}C_5H_{10} + H \Rightarrow C_5H_9 + H_2$	2.800e+13	4015.30
$C_2H_2 + O \Longleftrightarrow HCCO + H$	5.059e+06	1570.27	${}_1\text{-}C_5H_{10} + O \Rightarrow C_5H_9 + OH$	2.540e+05	−1123.33
$C_2H_3(+M) \Longleftrightarrow C_2H_2 + H(+M)$	2.000e+14	39744.26	${}_1\text{-}C_5H_{10} + OH \Longleftrightarrow C_5H_9 + H_2O$	6.800e+13	3059.27
$C_2H_2 + H \Longleftrightarrow C_2H_2 + H_2$	1.200e+13	0.00	${}_1\text{-}C_6H_{13} \Rightarrow {}_p\text{-}C_4H_9 + C_2H_4$	2.500e+13	28776.29
$C_2H_2 + O_2 \Longleftrightarrow CH_2O + HCO$	1.700e+29	6493.79	${}_1\text{-}C_7H_{15} \Rightarrow {}_1\text{-}C_5H_{10} + C_2H_5$	4.000e+13	28776.29
$C_2H_2 + O_2 \Longleftrightarrow CH_2CHO + O$	3.500e+14	5258.13	${}_1\text{-}C_7H_{15} \Rightarrow {}_1\text{-}C_4H_8 + {}_n\text{-}C_3H_7$	2.000e+13	28776.29
$C_2H_2 + O_2 \Longleftrightarrow C_2H_2 + HO_2$	5.190e+15	3307.84	${}_1\text{-}C_7H_{15} \Rightarrow {}_p\text{-}C_4H_9 + C_3H_6$	2.000e+13	28776.29
$C_2H_2 + O_2 \Longleftrightarrow C_2H_2 + HO_2$	2.120e 06	9474.19	${}_2\text{-}C_{10}H_{21} \Rightarrow {}_1\text{-}C_7H_{15} + C_3H_6$	1.500e+13	28274.38
$CH_3CO \Longleftrightarrow CH_3 + CO$	2.320e+26	17949.33	${}_3\text{-}C_{10}H_{21} \Rightarrow {}_1\text{-}C_6H_{13} + {}_1\text{-}C_4H_8$	1.500e+13	28274.38
$CH_3CHO + H \Longleftrightarrow CH_3CO + H_2$	2.100e+09	2413.96	${}_n\text{-}C_{10}H_{22} + OH \Rightarrow {}_3\text{-}C_{10}H_{21} + H_2O$	1.300e+07	−764.82
$CH_3CHO + H \Longleftrightarrow CH_2CHO + H_2$	2.000e+09	2413.96	${}_n\text{-}C_{10}H_{22} + OH \Rightarrow {}_2\text{-}C_{10}H_{21} + H_2O$	1.300e+07	−764.82
$CH_3CHO + OH \Longleftrightarrow CH_3CO + H_2O$	2.300e+10	−1123.33	${}_n\text{-}C_{10}H_{22} + H \Rightarrow {}_3\text{-}C_{10}H_{21} + H_2$	4.500e+07	4995.22
$CH_3CHO + CH_3 \Longleftrightarrow CH_3CO + CH_4$	2.000e−06	2461.76	${}_n\text{-}C_{10}H_{22} + H \Rightarrow {}_2\text{-}C_{10}H_{21} + H_2$	4.500e+07	4995.22
$C_2H_4 + H \Longleftrightarrow C_2H_3 + H_2$	5.400e+14	14913.96	${}_2\text{-}C_{10}H_{21} \Longleftrightarrow {}_3\text{-}C_{10}H_{21}$	2.000e+11	18116.63

and 11 vol.% aromatics. Flow rates of kerosene, oxygen, and nitrogen were adjusted to 1.06 cm^3/s, 10.30 cm^3/s, and 24.60 cm^3/s, respectively. The equivalence ratio was kept at 1.7. In simulation, the reactants are composed of 3.2%

n-decane, 28.57% O_2, and 68.23% N_2 (mole fraction). The mass flow rate of cold gas is 10.74×10^{-3} g/(cm^2 s).

As shown in Fig. 2a, the mole fractions of reactants, e.g., O_2 and *n*-decane, computed by the detailed and reduced mechanisms are identical. As compared with experimental data, the profile of O_2 mole fraction is predicted well with the reduced mechanism; however, a little discrepancy in quantity is observed at the same time. It may be caused by the lower actual flow rate of O_2 during experiment compared to the consumption rate of computed determined from the detailed reaction mechanism. It deserves to be noted that most of the measured small species are predicted very well, as demonstrated in Fig. 2b–h. The exceptions are found on CH_4, C_3H_6, and C_3H_4, which are under-predicted by approximate an order of magnitude in mole fraction. The mole fractions of most of the small species given by the reduced reaction mechanism are essentially consistent with those predicted by the detailed reaction mechanism except for those species, e.g., C_5H_{10} and C_6H_{12}. More interestingly, it is found that the profile of C_6H_{12} mole fraction is predicted better from the reduced mechanism than the detailed reaction mechanism in comparison with the experimental data.

From above discussions, we can found that this reduced reaction mechanism can provide a good prediction of the ignition and combustion characteristics of surrogate fuel *n*-decane. Thus, in the next sections, we will simulate the combustion process in an individual flame tube of one type of heavy duty gas turbine combustor using this reduced reaction mechanism.

Physical and computational models

The heavy duty gas turbine is a type of high efficiency and clean power engine, which is widely used in aero power generation. In this paper, the combustion process in the individual flame tube of one type of heavy duty gas turbine combustor is studied. The schematic of the individual flame tube used for numerical simulation is shown in Fig. 3. It consists of several sections including cyclone, spray nozzle, five intake annuluses, and outlet section. The structure of this flame tube is modified in order to reduce the computational cost. The primary combustion holes and mixing holes are abscised and five intake annuluses replaced the cooling gas film. Fuel is introduced through the central position of the triaxial tri-propellant injector and swirled using a tangential swirl nut, whereas air is injected through the leading section and five intake annuluses, respectively. The injector used in the modeled swirl-stabilized combustor is a general swirl-cup type of liquid fuel injector operated at the atmospheric pressure. It provides pressurized atomization and dual-radial, counter-swirling co-flows of air to disperse the fuel, and thus promotes fracturing of droplet as well as enhanced mixing.

The computing mesh of this individual flame tube is shown in Fig. 4. The mesh scales of the individual flame tube head and before the second intake annulus are 1 mm, others are 2 mm. The grid and node number are 437238 and 81649, respectively.

In the individual flame tube, a fixed mass flow rate boundary condition is imposed at the flow inlet. The inlet flow rate of fuel is set as 0.0032 kg/s and the inlet total flow rate of air is 0.2273 kg/s. The flow rates of air in each intake annulus are shown in Table 2. The initial temperatures of both inlet air and fuel are 300 K. The outlet boundary condition is considered as pressurized outlet boundary condition and the outlet pressure is kept at 1 atm.

Results and discussions

In this section, both the flow and the combustion processes in the individual flame tube are calculated. For comparison purpose, two typical surrogate fuels for kerosene are chosen, i.e., $C_{12}H_{23}$ and *n*-decane (*n*-$C_{10}H_{22}$). Fuel $C_{12}H_{23}$ has been listed in the fuel database of the CFD software (FLUENT) as the surrogate fuel of kerosene, and the reaction mechanism of this surrogate fuel in the reaction mechanism database of this software is one step reaction mechanism as $C_{12}H_{23} + 17.75O_2 \Rightarrow 12CO_2 + 11.5H_2O$ (pre-exponential constant A is 2.587×10^9, temperature exponent β is 0, and the activation energy E is 1.257×10^5 J/mole). But for surrogate fuel *n*-decane, a reduced reaction mechanism with 50 species and 210 elementary reactions is adopted, which is discussed above.

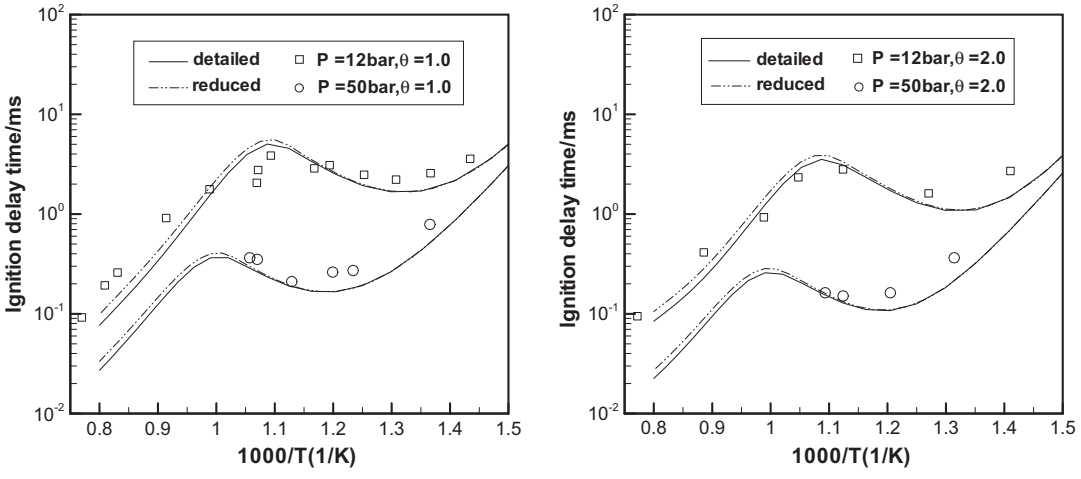

Fig. 1 Comparisons of computed (detailed and reduced mechanisms) and experimental ignition delay time in a shock tube reactor (full lines: detailed mechanism; double dotted lines: reduced mechanism; points: experimental data [18]).

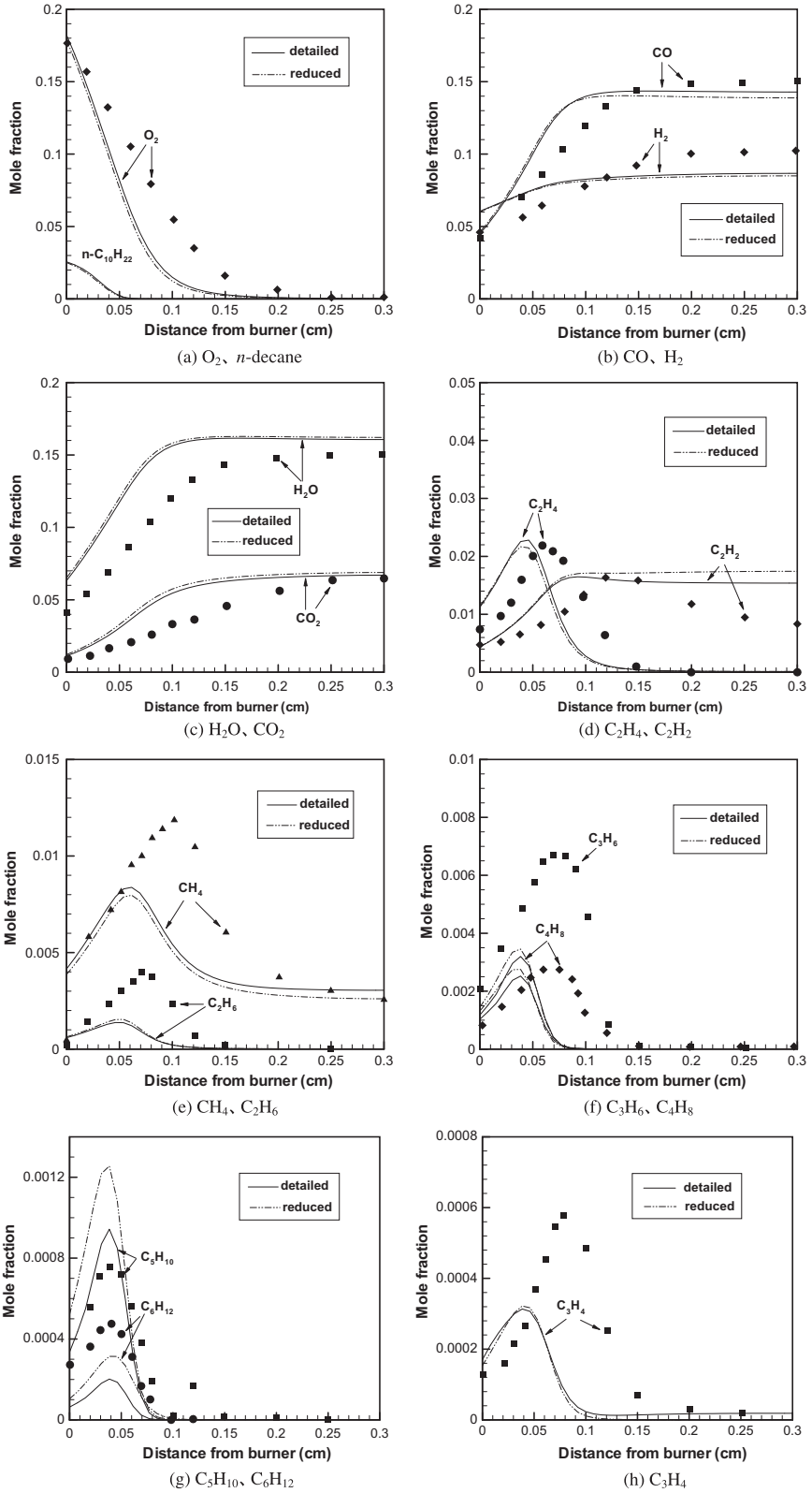

Fig. 2 The mole fractions of the main reactants and products. (Symbols designate experimental data [22], double dotted lines and the solid lines designate the profiles given by the reduced reaction mechanism and the detailed reaction mechanism, respectively).

Fig. 5 shows the computed scalar contour for flow field in the individual flame tube. The swirling air jets are merged together and expanded radially as they propagate downstream. Such radial expansion of high momentum air jets creates two

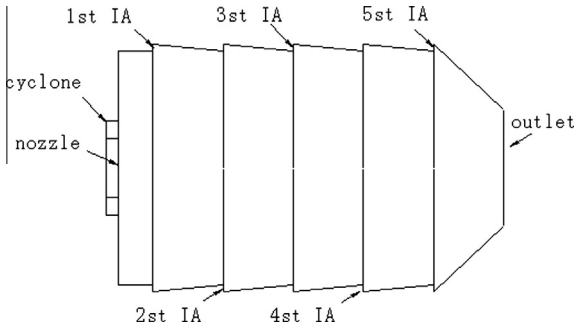

Fig. 3 Sketch of the individual flame tube (IA: intake annulus).

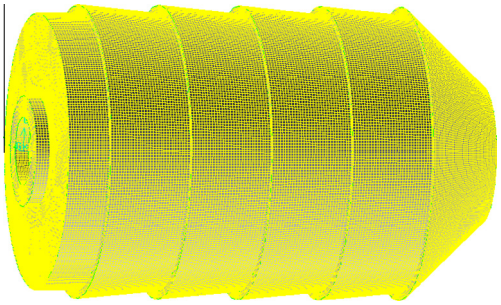

Fig. 4 Computational mesh of the individual flame tube.

toroidal recirculation regions: one at the corner and the other in the center. Interestingly, as compared with the results from one step reaction mechanism for surrogate fuel $C_{12}H_{23}$, the length of the center recirculation zone increased by using the reduced reaction mechanism for surrogate fuel *n*-decane. The possible reason may be the different physical characteristics of the two surrogate fuels. In addition, an increase in the length of the center recirculation zone might contribute to the additional formation of pollutants due to the increase in residence time.

The combustion characteristics associated with the two different surrogate fuels for kerosene are shown in the figures from Figs. 6–10. As can be observed in Fig. 6a, the flame of surrogate fuel $C_{12}H_{23}$ is anchored in the two regions, such as the corner recirculation region and the v-shaped region around the center zone, with a peak flame temperature around 2300 K. Compared with the surrogate fuel $C_{12}H_{23}$, the overall temperature in the flame tube is lower, although the temperature distribution shape is similar, when computed using *n*-decane fuel, as shown in Fig. 6b. It may be possibly caused by two reasons. One lies in the difference of underlying heat loss of vaporizing liquid droplets, as depicted in Fig. 7, the concentration contours of these two surrogate fuels in the flame tube. Due to the lower vaporizing rate of fuel $C_{12}H_{23}$ than that of *n*-decane fuel, the length of the fuel $C_{12}H_{23}$ jet appears to be longer than that of *n*-decane. Moreover, the concentration of *n*-decane in the center region is too low to provide enough fuel for combustion. So, as shown in Fig. 6b, temperature in this region is very low. The other reason may be the reaction mechanism adopted. When adopting fuel $C_{12}H_{23}$, one step reaction mechanism is used, and the fuel is completely combusted and the heat is released entirely. But in the case of *n*-decane, light hydrocarbons will be formed through the fuel pyrolysis reactions during combustion, e.g., $n\text{-}C_{10}H_{22} \Rightarrow 2_1\text{-}C_5H_{11}$, $n\text{-}C_{10}H_{22} \Rightarrow {}_p\text{-}C_4H_9 + {}_1\text{-}C_6H_{13}$, $n\text{-}C_{10}H_{22} \Rightarrow n\text{-}C_3H_7 + {}_1\text{-}C_7H_{15}$ and in the consequent reactions of these light hydrocarbons at low temperature and high temperature, as shown in Fig. 8. The heat will be released gradually achieving an homogeneously overall temperature in the individual flame tube.

Figs. 9 and 10 show the simulated concentration contours of the full combustion product, e.g., CO_2, as well as the intermediate species, e.g., CO, H, O, OH in the individual flame tube. It is worth noting that the concentration of CO_2 is higher in the high temperature region, as shown in Figs. 6a and 9a, as adopt $C_{12}H_{23}$ and the one reaction step mechanism. Addition-

Table 2 Intake gas quantity distributions of the swirler and intake gas annulus.

No.	Flow rate (kg/s)	No.	Flow rate (kg/s)
First intake gas annulus	0.0443	Fourth intake gas annulus	0.0443
Second intake gas annulus	0.0443	Fifth intake gas annulus	0.0414
Third intake gas annulus	0.0443	Swirler	0.0088

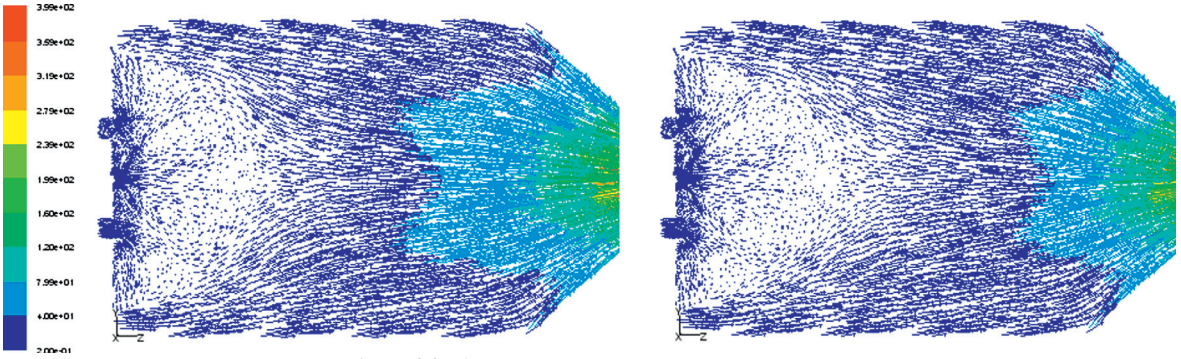

(a) one step reaction of fuel $C_{12}H_{23}$ (b) reduced reaction mechanism of *n*-decane

Fig. 5 Vector diagram in the individual flame tube (m/s).

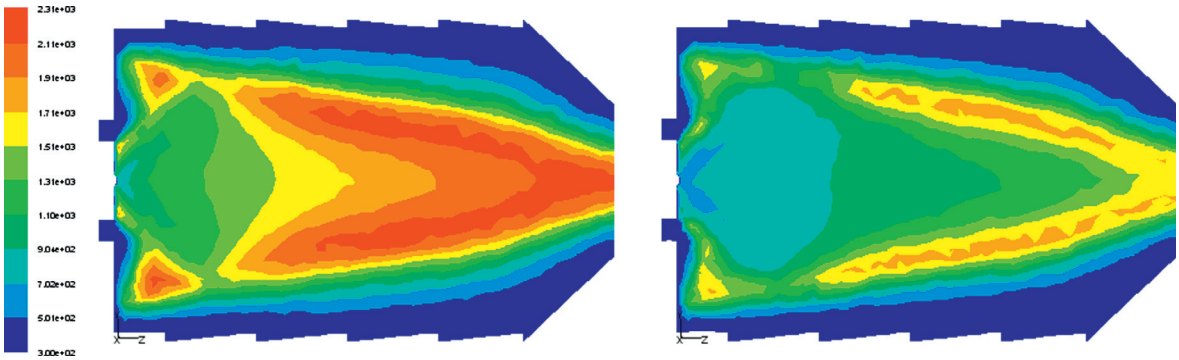

(a) one step reaction of fuel $C_{12}H_{23}$ (b) reduced reaction mechanism of *n*-decane

Fig. 6 Distribution of temperature (K) in the individual flame tube.

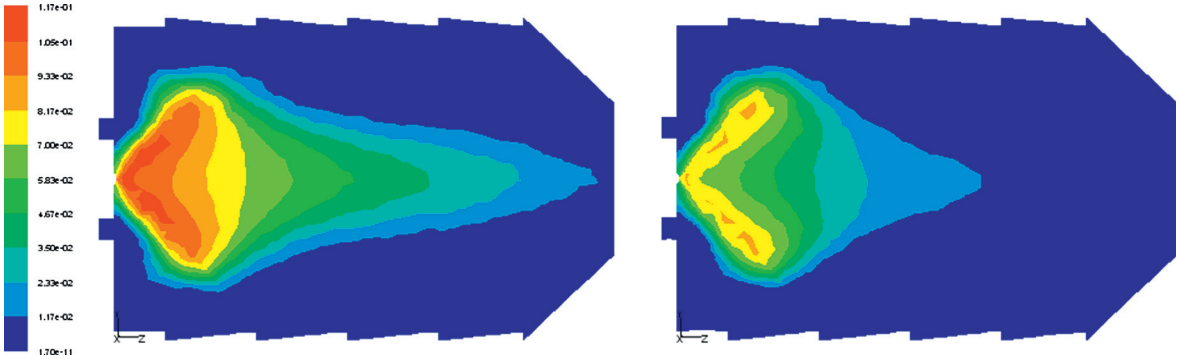

(a) one step reaction of fuel $C_{12}H_{23}$ (b) reduced reaction mechanism of *n*-decane

Fig. 7 Mole fraction distributions of fuel in the individual flame tube.

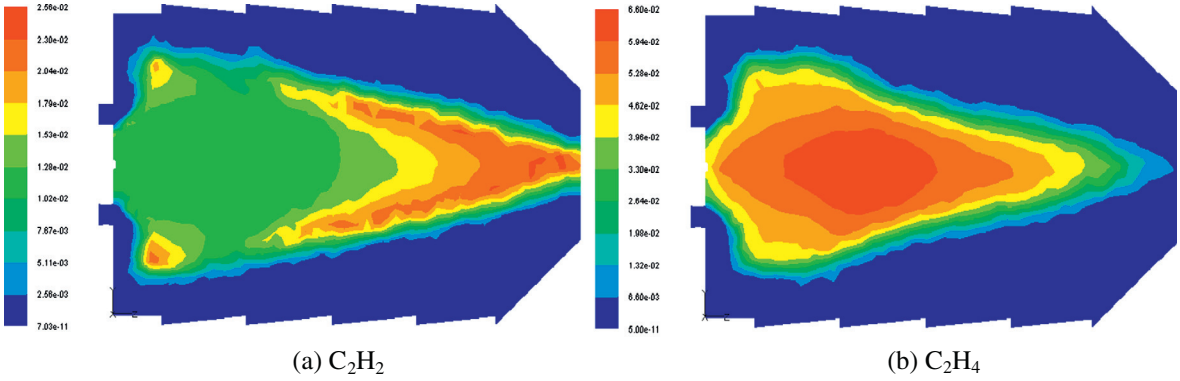

(a) C_2H_2 (b) C_2H_4

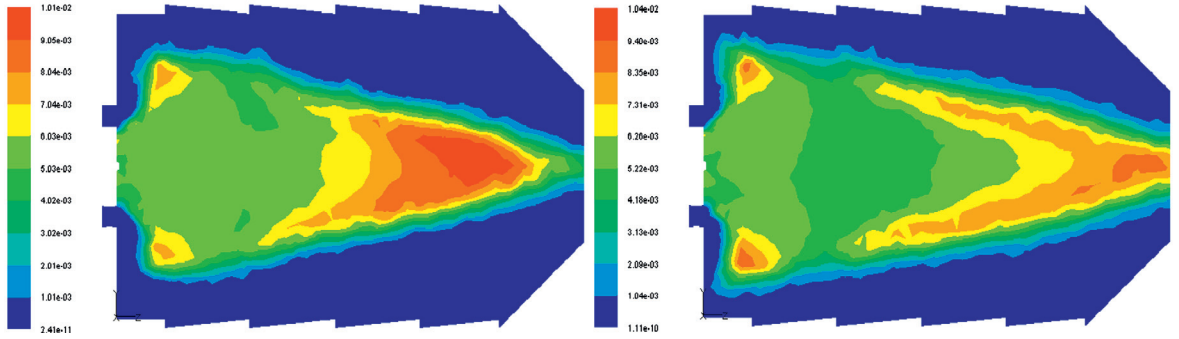

(c) CH_4 (d) C_4H_4

Fig. 8 Mole fraction distributions of C_2H_2, C_2H_4, CH_4 and C_4H_4 in the individual flame tube for reduced reaction mechanism of *n*-decane.

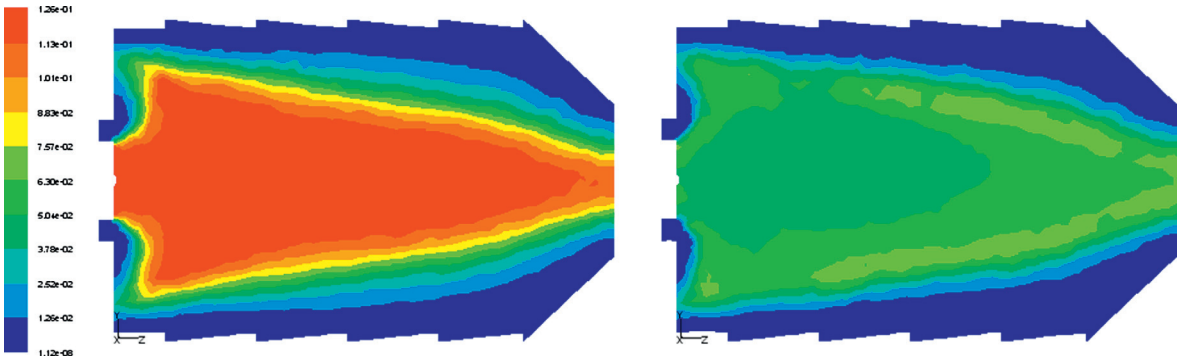

(a) one step reaction of fuel $C_{12}H_{23}$ (b) reduced reaction mechanism of *n*-decane

Fig. 9 Mole fraction distributions of CO_2 in the individual flame tube.

ally, no CO species formed during combustion and overall reaction products are CO_2 and H_2O. However, for *n*-decane and the reduced reaction mechanism, CO is only an intermediate species during fuel pyrolysis process. When there is enough amount of O_2 for fuel complete combustion, CO once formed will be rapidly converted to CO_2. But if the fuel is partially combusted, CO cannot be entirely converted to CO_2 as a result high concentration of CO will remain in the flame tube. It can be seen in Figs. 9b and 10a, the high concentration of CO_2 is achieved only in the V-shape high temperature region. In the center region, as shown in Fig. 6b, the concentration of CO_2 is found to be lower in low temperature region than high temperature region while the concentration of CO is relatively high.

The active species, e.g., H, O, and OH play an important role in combustion process. These intermediate species will activate the fuel combustion. As can be observed in Figs. 6b and 10b–d, the concentrations of H, O, and OH are high in the V-shape high temperature region.

Conclusions

A new reduced mechanism for surrogate fuel *n*-decane is developed. The aim is to retain only a small number of chemical species and reactions without losing accuracy. The predicted ignition delay times and the main reactants and main products mole fractions by this reduced mechanism agree well with experimental data.

By coupling this reduced reaction mechanism into CFD software, the combustion process in the individual flame tube of a heavy duty gas turbine combustor is kinetic simulated. For comparison purpose, another surrogate fuel $C_{12}H_{23}$, whose combustion process in the individual flame

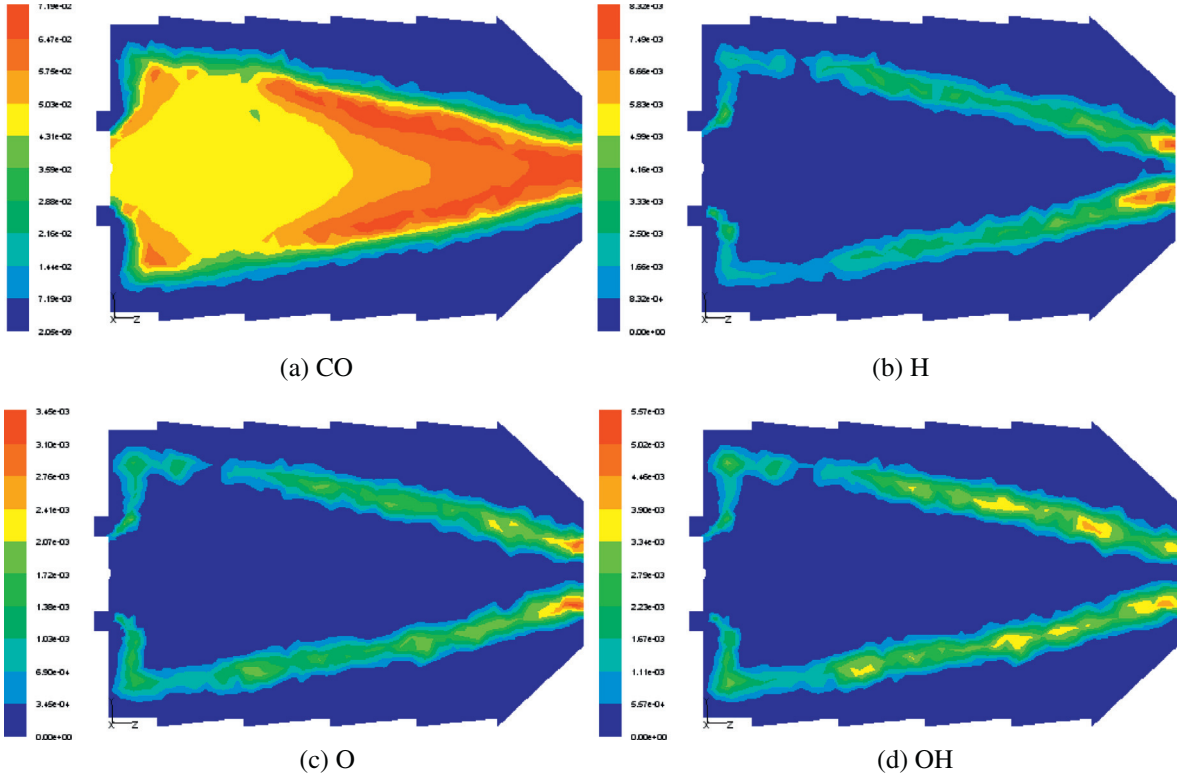

(a) CO (b) H

(c) O (d) OH

Fig. 10 Mole fraction distributions of CO, H, O and OH in the individual flame tube for reduced reaction mechanism of *n*-decane.

tube is also simulated, and one step reaction mechanism for this surrogate fuel combustion is adopted. There are a little of discrepancies in the flow and combustion processes of the individual flame tube adopting these two surrogate fuels, respectively.

(1) Compared with the results computed by one step reaction mechanism for surrogate fuel $C_{12}H_{23}$, the length of the center recirculation zone in the flow field in the individual flame tube increased, and the overall temperature in the flame tube is lower, although the temperature distribution shape is similar by adopting fuel *n*-decane.
(2) When adopting fuel $C_{12}H_{23}$, the concentration of CO_2 is high in the high temperature region. However, when adopting fuel *n*-decane, the high concentration of CO_2 is only in the V-shape high temperature region, and the concentration of CO is high in the center region.
(3) One step reaction mechanism can not reflect the effect of intermediate or active species such as H, O, OH on the combustion process of surrogate fuel. When adopting fuel *n*-decane and the reduced reaction mechanism is used, in the V-shape high temperature, the concentrations of H, O, OH are also high.

From the above discussions, it can be concluded that the simulated ignition and combustion characteristics of the surrogate fuel *n*-decane from adopting this new reduced reaction mechanism agrees well with experimental data. It also shows that this mechanism can be employed to predict the ignition and combustion of kerosene. This reduced reaction mechanism of fuel *n*-decane exhibits clear advantages in the simulation of the ignition and combustion processes in the individual flame tube over the one step reaction mechanism of fuel $C_{12}H_{23}$. Unfortunately, direct comparisons between the calculations and experiments are very limited since few published experimental data are available upon the simple laboratory flames of kerosene in the individual flame tube.

Conflict of interest

The authors have declared no conflict of interest.

Acknowledgement

The authors appreciate the financial support from the National Natural Science Foundation of China (50906059).

References

[1] Wang TS. Thermophysics characterization of kerosene combustion. J Thermophys Heat Transfer 2001;15:140–7.
[2] Dagaut P, Bakali AE, Ristori A. The combustion of kerosene: experimental results and kinetic modeling using 1- to 3-component surrogate model fuels. Fuel 2006;85:944–56.
[3] Saffaripour M, Zabeti P, Dworkin SB, Zhang Q, Guo H, Liu F, et al. A numerical and experimental study of a laminar sooting coflow Jet-A1 diffusion flame. Proc Combust Inst 2011;33:601–8.
[4] Honnet S, Seshadri K, Niemann U, Peters N. A surrogate fuel for kerosene. Proc Combust Inst 2009;32:485–92.
[5] Vovelle C, Delfau JL, Reuillon M. Formation of aromatic hydrocarbons in decane and kerosene flames at reduced pressure. In: Bockhorn H, editor. Soot formation in combustion: mechanisms and models. Berlin: Springer; 1994.
[6] Lindstedt P, Maurice LQ. Detailed chemical-kinetic model for aviation fuels. J Propul Power 2000;16:187–95.
[7] Cathonnet M, Voisin D, Etsouli A, Sferdean C, Reuillon M, Boettner JC. Kerosene combustion modelling using detailed and reduced chemical kinetic mechanisms. In: Symposium applied vehicle technology panel on gas turbine engine combustion, vol. 14. RTO meeting proceedings, NATO res. and tech. organisation, Neuilly sur seine, France, 1999. p. 1–9.
[8] Dagaut P, Ristori AE, Bakali A, Cathonnet M. Experimental and kinetic modeling study of the oxidation of n-propylbenzene. Fuel 2002;81:173–84.
[9] Patterson PM, Kyne AG, Pourkhashanian M, Williams A, Wilson CW. Combustion of kerosene in counter-flow diffusion flame. J Propul Power 2000;16:453–60.
[10] Cathonnet M, Guéret CB, Chakir A, Dagaut P, Boettner JC, Schultz JL. On the use of detailed chemical kinetics to model aeronautical combustors performances. In: Proceedings of the third European propulsion forum, EPF91, ONERA Paris, AAAF, 1992.
[11] Dagaut P, Reuillon M, Boettner JC, Cathonnet M. Kerosene combustion at pressures up to 40 atm: experimental study and detailed chemical kinetic modeling. Proc Combust Inst 1994;25:919–26.
[12] Luche J, Reuillon M, Boettner JC, Cathonnet M. Reduction of large detailed kinetic mechanisms: application to kerosene/air combustion. Combust Sci Technol 2004;176:1935–63.
[13] Leclerc FB, Fournet R, Glaude PA, Judenherc B, Warth V, Côme GM, et al. Modelling of the gas-phase oxidation of n-decane from 550 to 1600 K. Proc Combust Inst 2000;28:1597–605.
[14] Guéret CB, Cathonnet M, Boettner JC, Gaillard F. Experimental study and kinetic modeling of higher hydrocarbon oxidation in a jet-stirred flow reactor. Energy Fuel 1997;l6:189–94.
[15] Delfau JL, Bouhria M, Reuillon M, Sanogo O, Akrich R, Vovelle C. Experimental and computational investigation of the structure of a decane–O_2–Ar flame. Proc Combust Inst 1990;23:1567–75.
[16] Zeppieri SP, Klotz SD, Dryer FL. Modeling concepts for larger carbon number alkanes: a partially reduced skeletal mechanism for n-decane oxidation and pyrolysis. Proc Combust Inst 2000;28:1587–95.
[17] Nehse M, Warnatz J, Chevalier C. Kinetic modeling of the oxidation of large aliphatic hydrocarbons. Proc Combust Inst 1996;26:773–80.
[18] Bikas G, Peters N. Kinetic modelling of *n*-decane combustion and auto-ignition. Combust Flame 2001;126:1456–75.
[19] Bradley D, Habik SED, Sherif SA. A generalization of laminar burning velocities and volumetric heat release rates. Combust Flame 1991;87:336–46.
[20] Li G, Rabitz H. A general analysis of approximate lumping in chemical kinetics. Chem Eng Sci 1990;45:977–1002.
[21] Vlachos DG. Reduction of detailed kinetic mechanisms for ignition and extinction of premixed hydrogen/air flames. Chem Eng Sci 1996;51:3979–93.
[22] Douté C, Delfau JL, Akrich R. Chemical structure of atmospheric pressure premixed *n*-decane and kerosene flames. Combust Sci Technol 1995;106:327–44.